Detection of IR and sub/THz radiation using MCT thin layer structures: design of the chip, optical elements and antenna pattern

F.F. Sizov[1], Z.F. Tsybrii[1], V.V. Zabudsky[1], M.V. Sakhno[1], A.V. Shevchik-Shekera[1], S.Ye. Dukhnin[1], A.G. Golenkov[1], E. Dieguez[2], S.A. Dvoretsky[3]

[1]*V. Lashkaryov Institute of Semiconductor Physics, NAS of Ukraine,*
41, prospect Nauky, 03680 Kyiv, Ukraine
[2]*Universidad Autonoma de Madrid, Cantoblanco, 28049 Madrid, Spain*
[3]*A.V. Rzhanov Institute of Semiconductor Physics, RAS,*
pr. Lavrentieva, 13, Novosibirsk, Russia, 630090

Abstract. Two-color un-cooled narrow-gap MCT (mercury-cadmium-telluride) semiconductor thin layers, grown by liquid phase epitaxy or molecular beam epitaxy methods on high resistivity CdZnTe or GaAs substrates, with bow-type antennas were considered both as sub-terahertz direct detection bolometers and 3...10-micrometer infrared photoconductors. Optical system with aspheric THz lenses were designed and manufactured. An antenna pattern of structures on the thick substrate was discussed, and sensitivity of detector in both IR and sub-THz regions was measured.

Keywords: MCT, un-cooled two-color detector, antenna pattern.

1. Introduction

Over the past two decades, intense researches and development activities in academia and industry try to close the gap between the microwave and infrared spectra [1]. Compact terahertz sources and detectors are under development to generate, detect and manipulate coherent THz signals. Terahertz (THz) imaging and sensing technologies are increasingly being used in a host of medical, military, and security applications [2].

In spite of technology advancement in photonics, electronics and communications, the development of high-performance parts of vision systems, as well as of the systems as a whole, and their modeling and simulation will continue to be of interest for several reasons [3]. First, these parts are important system components for, as an example, surveillance and nonintrusive border security applications, standoff detection of explosives, and other military and security applications, since they qualify the system parameters. Second, development in the mentioned fields is likely to promote the design of more advanced THz vision systems. The development of THz imaging systems to provide the detectors, sources, and associated electronics capabilities is complex and costly. The design and manufacturing of them, especially un-cooled or slightly cooled parts, must be aimed at reducing the cost and extending application capabilities of THz vision systems. Compact detectors, both un-cooled and cooled but not below liquid nitrogen temperatures, powerful sources, and associated electronics are the key points that define the ultimate performance of THz imaging

systems, both passive and active. Modeling and simulation of these components (including, *e.g.*, matrix arrays and antenna simulation and optimization) are also an essential aspects. Further progress in physics-based modeling and simulation is important for developing better and cost-effective THz vision systems.

The key role in obtaining information about environment is played by detectors which should operate in different spectral ranges. It would be desirable to have detectors based on a small number of mature material technologies, or even, in ideal case, one material, thus restricting technologies of their manufacturing. However, realization of detectors based on few materials or even one material is a challenge because the physics of detector sensitivity in different spectral ranges are based on different physical phenomena and, as a rule, these different phenomena cannot be implemented within one material.

It was considered in [4] that such material as MCT semiconductor, the band-gap of which can be varied by altering the composition from $x = 1$ (CdTe band gap $E_g \approx$ 1.6 eV) to $x \approx 0.165$ (band gap $E_g \approx 0$ eV), can be applied as a sensitive element for infrared (IR) and sub-THz/THz detection. MCT is the material of choice for many IR focal plane array (FPA) applications. Characteristics of this semiconductor especially for the composition $x \approx 0.2...0.3$ were widely discussed, as they are suitable for $\lambda \sim 3...5$ and $8...12$ μm spectral regions photonic detectors, though they should be cooled, as a rule, to $T \approx 80...150$ K (see, *e.g.*, [5]). Important would be an expansion of MCT detector sensitivity to topical today THz/sub-THz electromagnetic radiation region. But tuning the chemical composition to x giving $E_g \Rightarrow 0$ (at $\nu \approx 1$ THz $h\nu \approx 4$ meV as compared to thermal energy ≈ 26 meV at room temperature) leads to high thermo-generation rate of carriers preventing an efficient THz/sub-THz detector operation based on interband optical transitions (photonic detectors).

The use of un-cooled MCT detector as THz with other detection mechanism compared to IR region was offered in [6], where the properties of a free electron gas heated by THz radiation were analyzed. Thus, there is an opportunity varying the characteristics of sensitive layers to apply such MCT detector technology for simultaneous operation in different spectral regions, which makes these systems more informative. Optical components design, as well as finding of 'good' antenna patterns are essential and should be done using proper materials.

## 2. MCT detectors architecture and experimental set-up

The design and dimensions of THz detector antennas were calculated for reasonable detector sensitivity within the 150...300-GHz frequency range. Under the influence of incident THz radiation, the changes in HEB (hot electron bolometer) sensitive element parameters take place at the length of several micrometers [6] and are much less compared to antenna dimensions, through which the radiation power is introduced to HEB. The antenna dimensions are conditioned by its effective area $A_{eff} = G\lambda^2/4\pi$ and are close to the wavelength λ, G is the antenna gain [7]. Here, it was chosen the simple bow-tie antenna with 90 ° divergence angle of side of antenna from the center of sensitive element. The electric contacts (narrow with width of 200 μm 10 times less than the radiation wavelength indium busses perpendicular to radiation polarization) were formed outside the antennas to reduce an influence on the antenna pattern. At the same time this construction of detector allows using symmetric and identical area current contacts (antenna blades) for photocurrent registration in IR spectral region. The photo of a single MCT HEB is shown in Fig. 1a. The horn, teflon lenses, scanning mirror, 8-element linear array of detectors and electronic board with circuits for detectors biasing, multiplexing and amplification of the output signals are shown in Fig. 1b.

To fabricate the detectors, there were used $Hg_{1-x}Cd_xTe$ ($x = 0.2...0.32$) layers grown using liquid-phase epitaxy (LPE) or molecular beam epitaxy (MBE) with the initial thickness of layers d from 5 to 20 μm. The technological route for manufacturing these structures consisted of the following stages: preliminary chemical preparation of MCT surface; formation of CdTe passivation layers; multilayered photolithographic processes; metallization by the lift-off photolithography or etching the mesa-structure methods to create planar contacts, samples cutting, bonding of samples for subsequent investigations.

a)
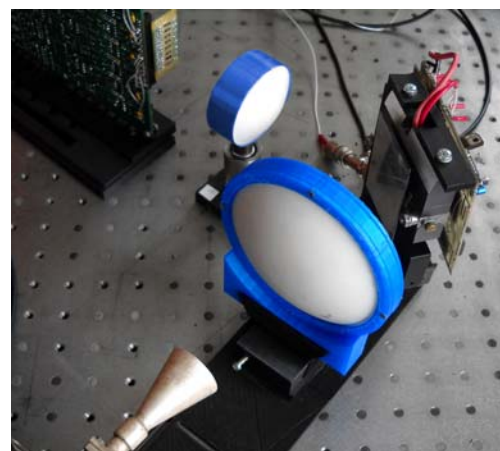
b)

Fig. 1. Photo of single MCT chip (a) and optical system with scanning mirror for THz imaging (b).
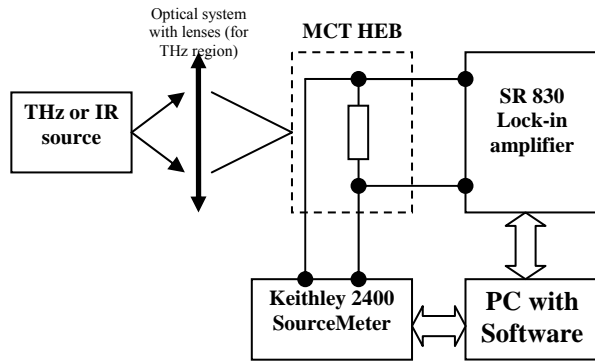
Fig. 2. Block-scheme of the test set-up.

Registration of signals from irradiated samples was carried out using the method of synchronous detection at changeable (up to 5 kHz) modulation frequency with use of Stanford Research SR-830 lock-in amplifier with internal noise ~6 nV/Hz$^{1/2}$. Continuous power on waveguide output was close to 25 mW. The IR photo-response was obtained using the globar with the temperature $T \approx 1600\,°C$ as a source of IR radiation and IR monochromator as a spectral instrument. As a dispersive element in the SPM-2 monochromator, a NaCl prism was used, and spectral resolution was $\Delta\lambda \leq 0.1$ µm. Detectors were current biased with $I_{bias} = 50...3000$ µA. The block-scheme of experimental set-up is presented in Fig. 2.

3. Modeling the antenna pattern on a thick substrate

MCT layers for detectors were grown on GaAs or CdZnTe substrates that have large permittivity. Substrates were thick (from ≈400 up to 800 µm), which was the reason of antenna pattern degradation. In earlier studies [8, 9], it was proposed to use electrically thin substrates (the substrate thickness $h < 0.1\lambda_d$, where λ_d is the wavelength inside the dielectric substrate). From the technological point of view, it is difficult to obtain thin substrates ($d \leq 60$ µm) when excitation of substrate modes can be excluded. There were investigated designs of antennas on thick substrates capable to operate with "good" antenna patterns.

The goal was to find constructions of antennas on thick substrates with patterns not strongly dependent on frequency, small changes of substrate dimensions and permittivity. Here, several approaches were considered:
1. Lenses on substrates (small lenses on the top of antennas).
2. Holes in substrates. Decreasing the substrate modes by making holes in substrates where electric field has maxima.
3. Adding conductive layer on the bottom of substrate, to make modes attenuate faster.

Table. Modeling parameters for the system with lens.

| System parameters		
Parameter	**Value**	**Description**
aAnt	1400 µm	Antenna length
aDet	100 µm	Length of the detector
aPad	400 µm	Pad length
aSub	6200 µm	Substrate length
aTot	5700 µm	Total length of antenna (with contact pads)
bAnt	700 µm	Antenna width
bCon	100 µm	Contact width
bDet	100 µm	Detector width
bPad	400 µm	Pad width
bSub	2000 µm	Substrate width
epsLayer	12.45	Permittivity of layer (thin layer between substrate and antenna)
epsLens	11.7	Relative permittivity of lens material
epsSub	10.89	Relative permittivity of substrate material
h2Lens	1000 µm	Height of cylindrical part
hLayer	8 µm	Thickness of layer
hLens	rLens	Height of spherical part of the lens
h2Lens	1000 µm	Height of cylindrical part of the lens
hSub	350 µm	Substrate thickness
rLens	1200 µm	Lens radius
sigmaLayer	3200 S/m	Conductivity of layer
sigmaLens	0	Conductivity of lens material
sigmaSub	0	Conductivity of substrate
aTot	110 µm	Printed antenna length
b1	50 µm	Printed antenna width
epsSub	9.36	Substrate relative permittivity
rHole	200 µm	Hole radius
xHole	500 µm	*x* coordinate of center of top-right hole
yHole	500 µm	*y* coordinate of center of top-right hole
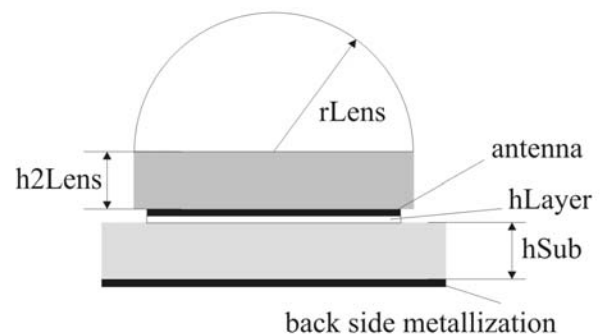
Fig. 3. The cross-section of the modeled system.

The system close to real was modeled to check lens operation. For modeling the antenna patterns, it was used the method of moments in the transmitting mode. The considered system was a rectangular substrate with length *a*Sub, width *b*Sub and thickness *h*Sub. The cross-section of antenna structure is presented in Fig. 3 (explanation of the symbols is cited in Table). On the top of substrate, there was a thin layer of conductive material (CdHgTe) with the thickness *h*Layer, relative permittivity epsLayer, conductivity sigmaLayer. On the top of these layers, the bow-tie antennas with contact pads were deposited. Back sides of substrates were metalized. All metals were approximated as perfect conductors. Hemispherical lenses with an additional part were located on the antenna. The radius of spherical part of lens was *r*Lens, height of cylindrical part was *h*2Lens. The parameters and their calculated values are presented in Table. Antenna patterns were calculated at 140 GHz frequency. Diameters of optimal lenses can be determined by modeling the different antenna structures. Dependences of antenna patterns on lens radius *r*Lens are shown in Fig. 4. As it follows from this figure, lenses begin to work starting from a 'critical' lens radius, and the antenna gain increases with lens radius.

Dimensions for lenses were designed taking into account two factors:
1. Large lens radius leads to larger gain.

2. Smaller lens radius leads to more compact position of the antennas.

It was found that the optimal lens radius should be slightly larger than the largest linear dimension of the antenna.

Concerning second approach for achieving "good" antenna pattern the idea was to make holes in the substrate to weaker modes in substrate and thus to decrease the level of side lobes. To check this assertion, we used a simple system: printed antenna on finite square substrate. Modeled system had the rectangular substrate with the length *LxSub*, width *LxSub* and thickness *h*Sub (Table). The backside of substrate was metallized. All metals were assumed to be perfectly conductive. The printed dipole antenna had the length *aTot* and width *b1* and was positioned in the substrate center. Holes in substrate had the radius *rHole* and were positioned symmetrically in respect to the substrate center. They were positioned in places where the equivalent surface current was maximal. If equivalent surface current is maximal, there is the maximum of electric field. Presence of the hole in that place makes excitation difficult. Comparing Fig. 5a and 5b shows that making holes is a way for creating better antenna pattern at one frequency. But at different frequencies, modes have different configuration and, as such, may not be in proper places.
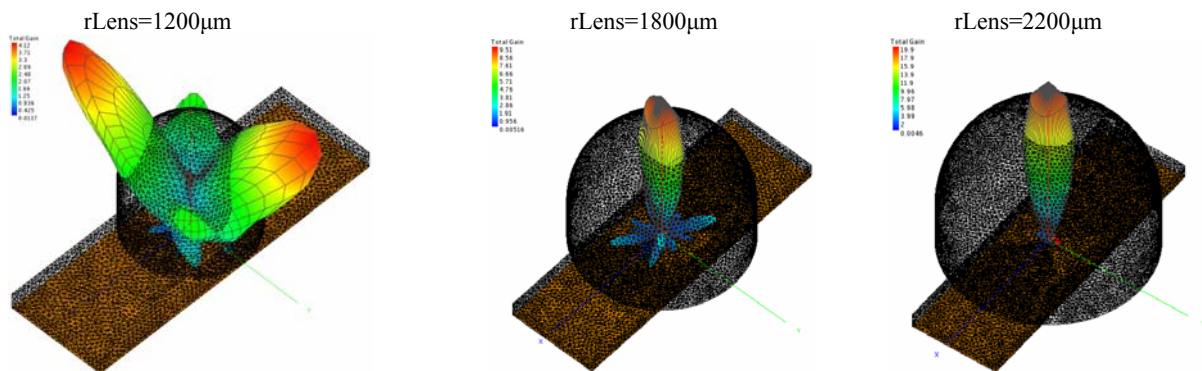
rLens=1200µm   rLens=1800µm   rLens=2200µm

Fig. 4. Calculated antenna patterns for different lens radius.

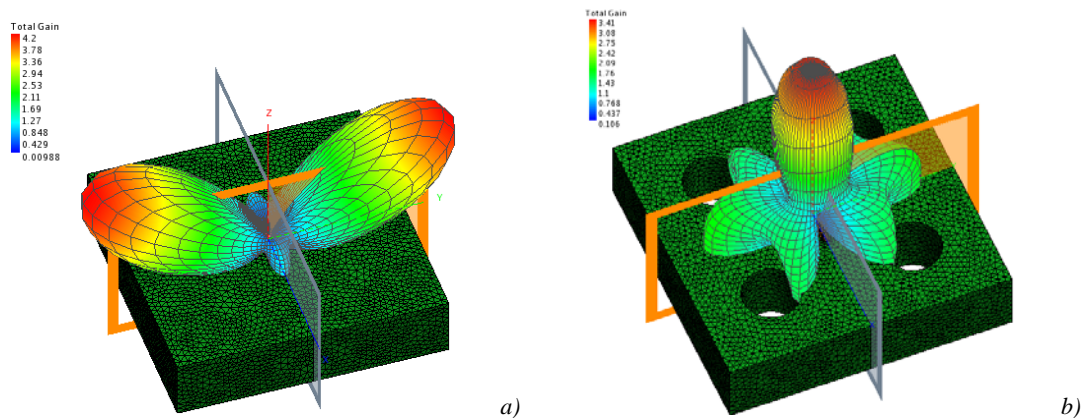*a)*   *b)*

Fig. 5. Antenna pattern for system without holes (a) and with holes (b) at the frequency 140 GHz.
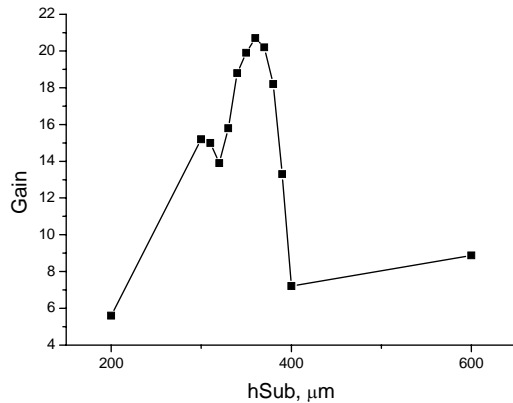
Fig. 6. Antenna gain in normal direction dependence on the substrate thickness for 140 GHz radiation frequency.

As for thickness of substrate, modeling the antenna gain in normal direction dependence on the substrate thickness was performed, and the result of simulation is shown in Fig. 6.

4. Optical system design and signal processing for the 8-element linear detector array

For inputting radiation into detectors and getting the image, one needs to use an optical system consisting of lenses or mirrors. Imaging with IR and especially THz waves is usually achieved using off-axis parabolic mirrors and aspherical lenses [10]. The off-axis parabolic mirrors are susceptible to aberrations once misaligned, and the alignment is always difficult as the direction of the optical axis changes upon reflection of the mirror. Lenses are much easier to align, they are less susceptible to aberrations, and allow higher numerical aperture (*NA*). Just placing the lenses into an optical axis with no tilt ensures proper alignment. While a parabolic surface is the only solution for a mirror to convert a plane wave front into an aspherical one, a lens with its two surfaces allows an infinite number of solutions.

An optical system includes a THz source for emitting radiation (140 GHz). The first pair of lenses focuses the light on the object; the second one focuses it to THz detector. Presented lenses were designed using Kirchhoff's scalar diffraction theory. Ultra-high molecular weight of polytetrafluoroethylene (PTFE) with the refractive index 1.43 within a wide wavelength region was selected as lens material. Aspherical lenses were chosen. The aspherical profile is more complex surface, as compared to the spherical one, and can reduce or eliminate spherical aberrations as well as decrease other optical aberrations, *e.g.*, astigmatism. A single aspheric lens can often replace much more complex multi-lens system. The resulting device is smaller and lighter, and sometimes cheaper than the multi-lens design. The diffraction limited optical system with four identical plane-convex aspherical lenses (hyperboloid) was designed and manufactured.

Lenses were milled on a computer-controlled lathe, and the resulting surface roughness was less than 30 μm (~λ/10). For all of the lenses used in active imaging system and studied here, the focal length 70 mm and diameter 60 mm were taken. The focal length of the lenses was determined using the paraxial part of the beam. A lens spot diagram is the best overall evaluation for a quick check of image quality. In the diffraction-limited case, the central circle is the Airy disk. Outside the Airy disk, light is diverted due to various aberrations. Calculated and experimentally measured by the manufactured MCT detector the diffraction point spread function (PSF) of the optical system have rather similar values ($D_{Airy-calc}$ = 5.6 mm, $D_{Airy-meas}$ ≈ 8 mm), that satisfactory confirms the quality of the lenses manufactured and their ability to be used for imaging. 3D image of the sub-THz beam (ν = 140 GHz) and one along the *x-y* axes as focused by an aspheric four-lenses optical system is shown in Fig. 7.
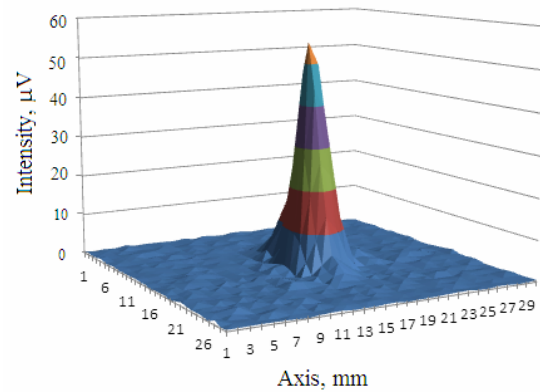
a)
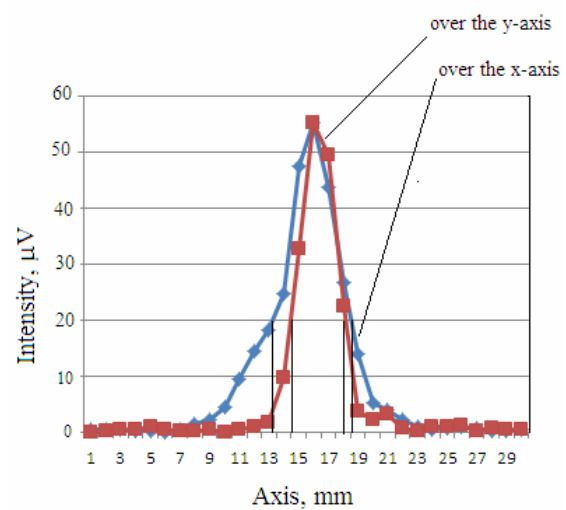
b)

Fig. 7. Measured by MCT bolometer 3-D spot diagram created by passing of THz beam through the optical system consisting of four aspheric lenses (a) and spot diagram along the *x* and *y* coordinates (b).

For imaging based on using the 8-element MCT HEB array, it is necessary to provide individual biasing for each element and subsequent amplification of its output signal up to the levels that can be digitized using external analog-to-digital converter. For this purpose, the electronic circuit board for the stabilized current (voltage) bias setting and two-stage signal amplification from the linear arrays was developed. Every detector's output signal is enhanced by input amplifier with the gain coefficient close to 20. Then, the amplified signal is transmitted to the control amplifier that is intended for eliminating the bolometer output voltage non-uniformity. Analog keys ensure functioning of the readout circuit in the modes of accumulation and storage of a charge, and also discharge of capacitive storage. An analog multiplexer supports serial interface of parallel input signals. The control circuit generates managing signals for the readout scheme.

5. IR/sub-THz MCT detectors responsivity

Mechanisms of MCT detector responsivity are different in IR and sub-THz spectral regions. In MCT IR photoconductor, the changes in conductivity rise under the IR illumination, which results in a photoconductor response due to valence-to-conductance band transitions (photonic detector) as in other intrinsic photoconductors. In MCT sub-THz/THz HEB, the response is caused by heating the electron gas with the power introduced via antenna and motion of free carriers in the sensitive element [6]. This motion is governed by three different effects, which under THz radiation can lead both to increase and to decrease the detector conductivity.

Here, the THz/sub-THz response of MCT detectors is observed in n-type layers with the electron concentration $n_{78K} \approx 2 \cdot 10^{14}$ cm^{-3} for the chemical composition $x \approx 0.216\ldots0.224$ and $5\ldots7$-μm layer thicknesses. The resistances of samples were approximately $300\ldots400$ Ohm. The detected at $T = 300$ K IR spectrum for one of the detectors is shown in Fig. 8.
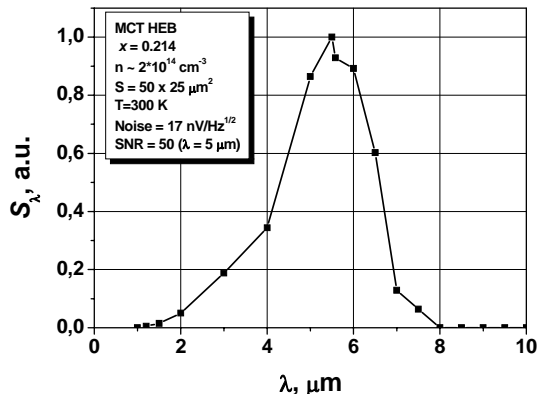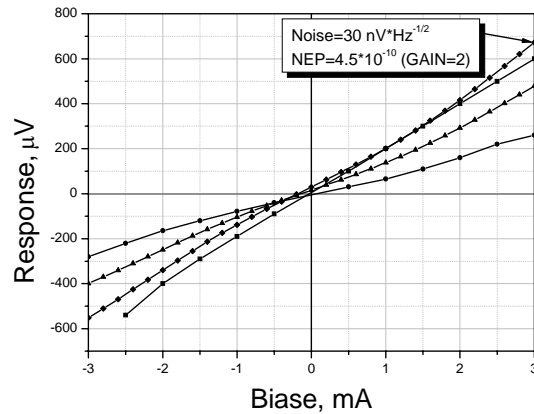
Fig. 9. Dependence of the response signal *vs* current through the sensitive element for 4 detectors from the 8-element MCT HEB array at $T = 300$ K and radiation frequency 140 GHz.

For these detectors used for sensing of sub-THz radiation at $\nu = 140$ GHz, the best measured noise equivalent power values were NEP$_{300K} \approx 4.5 \cdot 10^{-10}$ W/Hz$^{1/2}$. Fig. 9 shows the response signal *vs* current through sensitive element for 4 detectors from 8-element MCT HEB array at $T = 300$ K and radiation frequency 140 GHz. Noise-equivalent power was calculated for the best detector at 3-mA bias (Fig. 9). Experimentally measured noise at this bias was 30 nV·Hz$^{-1/2}$. As the internal noise of used SR-830 lock-in amplifier is 6 nV·Hz$^{-1/2}$, it is difficult to carry out the measurements of detector's noise at lower currents. In this type of detectors, the generation-recombination noise prevails at a non-zero bias and $T = 300$ K. Generation-recombination noise linearly depends on current through detector. It was the reason to measure noise at relatively high current to minimize the influence of intrinsic noise from experimental set-up. The observed responsivities were $R \sim 600$ V/W ($T = 300$ K).

6. Conclusions

Un-cooled MCT hot electron bolometer detectors with bow-tie antennas show the possibility to operate both in sub-THz and IR spectral ranges. Modeling the antenna patterns demonstrates that the optimal lens radius should be larger than the antenna's largest linear dimensions, and antenna gain increases with the lens radius. The system for possible THz-imaging consisted of the horn, teflon aspherical lenses, scanning mirror, 8-element linear array of detectors and electronic board with circuits for detectors biasing, multiplexing and amplification of the output signals have been designed and manufactured. For MCT detectors from array used for sensing of sub-THz radiation at $\nu = 140$ GHz, the measured noise was about 30 nV·Hz$^{-1/2}$ at 3-mA bias and corresponding noise equivalent power value was NEP$_{300K} \approx (4.5\ldots9) \cdot 10^{-10}$ W/Hz$^{1/2}$ that may be supposed as sufficient for active imaging.

Fig. 8. Responsivity spectrum S_λ of MCT detector in IR region at $T = 300$ K.

References

1. D. Saeedkia (Ed.), *Handbook of Terahertz Technology for Imaging, Sensing and Communications*. Oxford, Woodhead Publishing Series in Electronic and Optical Materials, Number 34, 2013.
2. G.J. Wilmink & J.E. Grund, Current state of research on biological effects of terahertz radiation // *J. Infrared Millimeter and Terahertz Waves*, **32**, p. 1074-1122 (2011), DOI:10.1007/s10762-011-9794-5.
3. C. Corsi and F. Sizov, *THz and Security Applications- Detectors, Sources and Associated Electronics for THz Applications*. Springer, The Netherlands, 2014.
4. F. Sizov, Z. Tsybrii, V. Zabudsky et al., Mercury–cadmium–telluride thin layers as subterahertz and infrared detectors // *Opt. Eng.* **54** (12), p. 127102-1–127102-8 (2015), doi:10.1117/1.OE.54.12.127102.
5. A. Rogalski, *Infrared Detectors* (2-nd ed.). Taylor & Francis, Boca Raton, New York, 2011.
6. V. Dobrovolski and F. Sizov, THz/sub-THz bolometer based on electron heating in a semiconductor wave-guide // *Opto-Electron. Rev.* **18**, p. 250-258 (2010).
7. J.L. Volakis (Editor), *Antenna Engineering Handbook*, 4th ed. McGraw-Hill Companies, New York, 2007.
8. D. Pozar, Considerations for millimeter wave printed antennas // *IEEE Trans. Antennas Propag.* **31**, p. 740-747 (1983).
9. M. Sakhno, J. Gumenjuk-Sichevska, F. Sizov, Modeling of the substrate influence on multielement THz detector operation // *J. Infrared, Millimeter, and Terahertz Waves*, **35**(9), p. 703-719 (2014).
10. S. Hunsche, M. Koch, I. Brener, and M.C. Nuss, THz near-field imaging // *Opt. Communs.* **150**, p. 22-26 (1998).